Impact of the dayglow and the Ring effect on the retrieval of surface pressure from the *A* and *B* bands of O_2: application to Orbiting Carbon Observatory

Christopher E. Sioris
Harvard-Smithsonian Center for Astrophysics

Executive summary- Retrievals of surface pressure from the O_2 *A* and *B* bands are performed at the spectral resolution of the Orbiting Carbon Observatory using "measured" radiances containing the spectral signature of the dayglow or rotational Raman scattering. However, the forward model used to simulate the radiances in the retrieval algorithm only includes elastic scattering and molecular absorption. The error in retrieved surface pressure is thus due to the neglect of airglow and Ring effect in the forward radiative transfer model. Despite significant fitting residuals in the cores of the *A* band lines, the retrieval of surface pressure is essentially immune (within 0.4 mb) to both of these atmospheric radiative transfer effects.

1. IMPACT OF *A* BAND DAYGLOW

1.1 Background: *A* band dayglow

Owing to its relatively short radiative lifetime of ~10 seconds [Gamache *et al.,* 1998] relative to the time scale of collisions in the upper atmosphere, O_2 molecules spontaneously emit radiation via the *A* band ($b^1\Sigma_g^+$- $X^3\Sigma_g^-$, 0←0) throughout the mesosphere and lower thermosphere. Daytime emissions are initiated through O_2 photolysis, O_2 resonance scattering, and ozone photolysis [Marsh *et al.*, 2002]. The *B* band (1←0) does not exhibit dayglow as its radiative lifetime is an order of magnitude longer (140 s, [Gamache *et al.,* 1998]) and the vibrational quantum of energy is collisionally quenched before radiative emission can occur [Abreu *et al.*, 1989].

The *A* band dayglow was first observed by Wallace and Hunten [1968]. Dayglow observations in nadir geometry have not appeared in the literature to the best of the author's knowledge, presumably due to the difficulty in interpreting these observations because of the strong absorption signature in the backscattered radiation upwelling from the lower atmosphere and surface. Satellite observations of the seasonal and latitudinal dependence of the *A* band daytime volume emission rate (VER) between 80 and 110 km have been first made by the High Resolution Doppler Imager (HRDI) onboard UARS [Marsh *et al.*, 1999] and recently [Marsh *et al.*, 2002], the analysis of HRDI *A* band dayglow was extended down to 65 km. A recent flight of the METEORS rocket [Mlynczak *et al.*, 2001] was also very successful in measuring the volume emission rate of the O_2 ($^1\Sigma$) and $O_2(^1\Delta)$ 0-0 bands between 65 and 95 km.

The impact of the dayglow on surface pressure retrievals from the O_2 *A* band in nadir geometry has never been studied previously. The purpose of this section is to quantify the errors in retrieved surface pressure due to neglecting the dayglow in the forward radiative transfer model of the retrieval algorithm. The bias and uncertainty of the surface pressure retrieval is sought to within a factor of two.

To determine the nadir spectral radiance due to the *A* band dayglow, limb radiances measured by the Optical Spectrograph and Infrared Imager System (OSIRIS) are used. OSIRIS and SCIAMACHY (Scanning Imaging Absorption Spectrometer for Atmospheric Chartography) are two recently launched satellite instruments that currently make vertically resolved *A* band day and nightglow measurements in limb viewing geometry with near-global coverage. OSIRIS is onboard the Odin satellite which has an equator crossing time of ~6 am at the descending node and a polar sun-synchronous orbit. The OSIRIS radiances (photons/cm^2/s/nm/sr) have been corrected for instrumental response and are thus absolutely calibrated in this respect. The measurements are on a ~2 km tangent height (TH) grid with a 1×40 km^2 instantaneous field-of-view (IFOV, vertical × horizontal) at the tangent point and range from the middle troposphere to the lower thermosphere (4-103 km) in stratospheric-mesospheric observing mode. The radiances (Figure 1a-b) show the signature of the *A*, *B*, and γ bands in absorption and, for high THs, the *A* band in emission at ~1 nm resolution and ~0.4 nm spectral sampling.

SCIAMACHY has an equator crossing time of 10 am at the descending node and a polar sun-synchronous orbit. Limb radiance spectra are recorded from –3 to ~100 km, sampled every 3.3 km with an IFOV of 2.6×110 km^2 at the tangent point. The spectral resolution at the *A* and *B* bands is ~0.48 nm (Bovensmann *et al.*, 1999) and the spectral sampling is ~0.21 nm. Limb scattering spectra from SCIAMACHY are shown in Figures 1c-d. It is clear upon comparing these two figures that the $^1\Delta$ (0←0) dayglow is much stronger relative to the scattered limb radiance. For example, the limb radiance in the $^1\Delta$ band (Figure 1c) at TH=50 km is greater than the radiance at a tangent height just above the surface (TH= 0.32 km). In the *A* band at SCIAMACHY resolution (Figure 1d), the radiance in the centre of the *R* branch is more than an order of magnitude larger the radiance at the TH with the strongest glow (i.e. TH= 89 km). This suggests the *A* band will be much more favourable for the retrieval of the column of O_2 by its absorption signature.

1.2 Method

1.2.1 Determining the nadir glow radiance spectrum from OSIRIS limb radiance spectra

The OSIRIS radiances were inverted into a vertical profile of volume emission rate (photons/cm^3/s) using an onion peel technique. First, the OSIRIS radiances were interpolated onto a 2-km TH grid (50-102 km). Scattering was removed by linearly interpolating the continuum on either side of the *A* band to each of the OSIRIS pixel centres within the *A* band. This interpolated continuum is subtracted from the limb radiance to give the observed limb radiance profile due to emission. An approximate correction is made for O_2 absorption along the line-of-sight (LOS) in the scattered radiance using transmittances calculated line-by-line (using a new, more versatile version of the McLinden *et al.* [2002] pseudo-spherical radiative transfer model) and binned according to the OSIRIS CCD pixel edges but convolution was neglected to improve computational speed. It is assumed that the scattering occurs entirely from the tangent point and that the solar spectral irradiance is constant over the *A* band. The importance of this correction is shown in Figure 2. Particularly for high SZAs, a correction for the O_2

absorption along other parts of the light path (i.e. incoming path) should be included as well. Air, O_2, ozone and temperature profiles for March, 55° N are assumed (McLinden *et al.*, 2002) for the transmittance calculation.

The observed limb glow radiance is modelled as follows. The absorption optical depth of O_2 along the line of sight to a given tangent height is used as the emission basis function for the tangent layer. This emission basis function is normalized to the emission basis function at 50 km. This yields a set of emission basis functions with equal wavelength-integrated radiance (photons/cm^2/s/sr) but each basis function is different spectrally because pressure broadening and temperature are functions of altitude. The emission basis functions are inexact in three ways:

1) In emission, the initial rotational state populations are actually the final state populations for absorption so the line intensities are only approximate
2) Non-LTE effects are also expected since collisional deactivation does not dominate, particularly above 95 km (Wallace and Hunten, 1968).
3) The emission basis function should be appropriate to the layer and not integrated along the line of sight. Thus the width of the lines and temperature for emission are only approximate.

Considering the sensitivity of the surface pressure retrieval to airglow determined below, such secondary effects are of trivial importance.

The retrieval algorithm consists of iteratively updating a scaling factor, $c_{E(z)}$, for the emission until the modelled and observed *A* band limb radiance (photons/cm^2/s/sr) are equal within the convergence criterion of 1% at all tangent heights. The updating is based on Chahine's [1970] relaxation method.

A path length matrix was developed for each 2 km vertical layer using spherical geometry. For the top layer of the retrieval (100-102 km), the transmittance is assumed to be 1 over the entire wavelength range of the *A* band. The modelled dayglow limb radiance for a given tangent height is equal to:

$$\int_{\lambda_1}^{\lambda_2} \left(\int_{z=TH}^{\infty} path(z,TH) \times I_{z,\lambda} \times c_{E(z)} \times T_{z\to\infty,\lambda} \, dz \right)^{\otimes} d\lambda \qquad (1)$$

where λ_1 and λ_2 define the fitting window (758.8-768.0 nm), $I_{z,\lambda}$ is the unit emitted spectral radiance at wavelength λ leaving altitude *z*, $T_{z\to\infty,\lambda}$ is the spectral transmittance from z to ∞ along the LOS, $c_{E(z)}$ is proportional to the volume emission rate in the z^{th} layer and $\otimes$ denotes the convolution operation and a FWHM of 16 cm^{-1} has been assumed (appropriate for OSIRIS in the *A* band) with a triangular instrument line shape. For underlying atmospheric shells, the transmittance of emitted radiation along the LOS is <1 due to various extinction sources: ozone and O_2 absorption, and Rayleigh scattering. The modelled glow radiance is the integral along the LOS (as in Eqn. 1, including both the far and near side). Note that resonance scattering is ignored in this treatment (i.e. O_2 molecules which absorb *A* band photons do not re-emit into the LOS).

Convergence was achieved down to 51-53 km for most profiles. Non-linearity due to strong O_2 self-absorption [Heller *et al.*, 1991] combined with sharply decreasing

sensitivity due to small volume emission (as a result of collisional quenching) limited the retrieval from progressing further down.

Once the inversion is complete, the A band VER profile is simply

$$VER(z) = 4\pi \int_{\lambda_1}^{\lambda_2} (c_{E(z)} \times I_\lambda)\, d\lambda \qquad (2)$$

The inverted VER profiles (Figure 3) compare favorably with HRDI measurements from March 1993 and with the results of Wallace and Hunten [1968] who found an approximately constant VER of 1e5 photons/cm^3/s between 70-90 km. The measured and modelled volume emission rates of Mlynczak *et al.* [2001] and Bucholtz *et al.* [1986], respectively, are also are in general agreement with these results.

The orbital variation (Figure 3) is a melange of latitudinal and diurnal variation. OSIRIS is very close to the day/night terminator, especially at this time of year, and thus the solar zenith angle (SZA) is almost constant (Figure 4). This assists in separating the latitudinal dependence from the SZA dependence. The use of OSIRIS data also allows the full diurnal variation to be resolved (sunrise to sunset) and allows greater geographic coverage than the HRDI measurements (82 vs. 72 N). Assuming an equator crossing time of 1:30 pm, OCO will rapidly transit through twilight over the poles and will likely see a diurnal dependence in the airglow intensity manifest itself as a latitudinal dependence.

The nadir glow spectral radiance ($I_{nad,\lambda}$) is given by

$$I_{nad,\lambda} = \frac{1}{4\pi} \int_{z=0}^{\infty} \mathrm{VER}_{z,\lambda}\ \mathrm{T}_{z\to\infty,\lambda}\ \mathrm{dz}$$

where $VER_{z,\lambda}$ is the spectral volume emission rate (photons/cm^3/s/nm). If $T_{z\to\infty,\lambda} \cong 1$ for all heights where $VER_{z,\lambda}>0$, then the nadir spectral radiance due to dayglow is simply the integral of $VER_{z,\lambda}$ over height divided by 4π steradians. This is the case for nadir transmittance, where even from 62 km, extinction along the nadir (LOS) path reduces the band-integrated transmission by only 10% (Figures 5a-b). The extinction is due primarily to self-absorption. The nadir glow radiance (integrated along the line of sight) is reduced by 8% assuming a volume emission rate profile for 12° N shown in Figure 3.

The nadir dayglow radiance over the northern hemisphere shown in Figure 6 has a standard deviation that is 15% of the mean (1σ=4.82e9 photons/cm^2/s/sr, 0=3.29e10 photons/cm^2/s/sr). This is the variability over the orbit without any orbital detrending of the glow. The absolute and relative variability as a function of altitude are shown in Figures 7a-b. The absolute variability increases almost monotonically with decreasing altitude. The relative variability (standard deviation divided mean) however tends to peak in the lower mesosphere (~71 km) where sharp gradients in ozone exist. At the secondary maximum of O_3, collisional excitation of O_2 by $O(^1D)$ (a product of ozone photolysis) leads to orbital variability in the dayglow intensity of the atmospheric 0-0 band. The following process is important for the sharp local enhancement near 88 km and in the lower mesosphere [Marsh *et al.*, 2002]:

$O_2\ (^3\Pi) + O^1D \rightarrow\ O_2(^1\Sigma) + O^3P$ (collisional excitation)

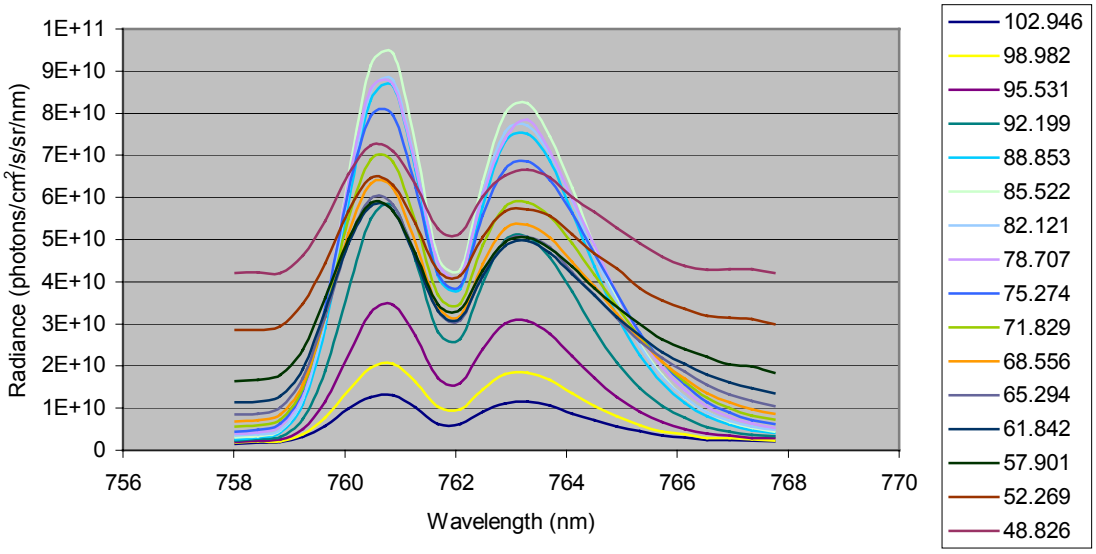

Figure 1a – OSIRIS limb radiance (61.9° N, SZA=84.4° pm, March 16th, 2002). Every second spectrum in the mesosphere is shown from this limb scan. The tangent height (km) of each spectrum is shown in the legend. Note that scattering raises the continuum at lower tangent heights. However, the spectral radiance is largest at the *R* branch core at 85.5 km.

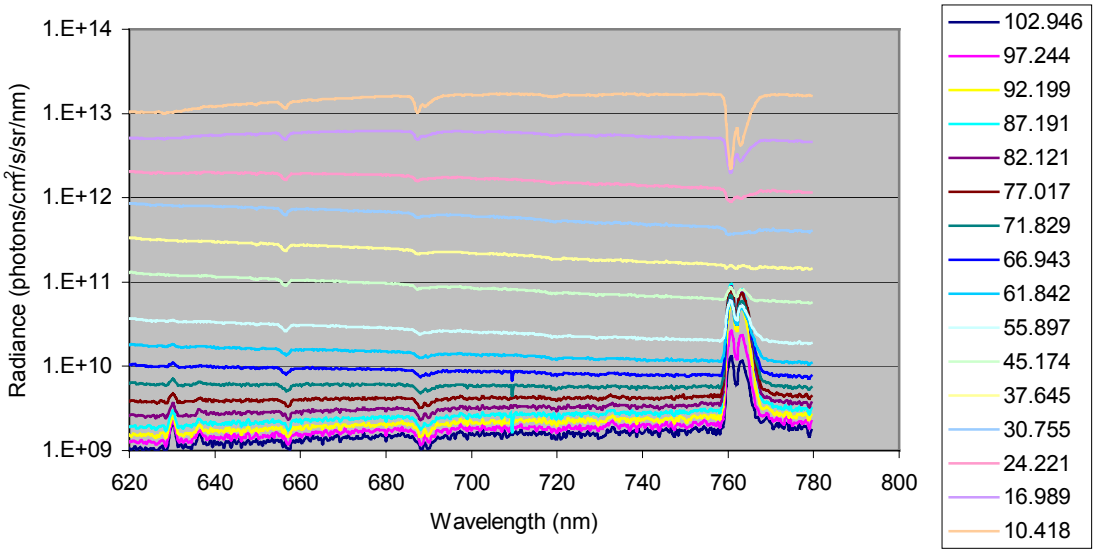

Figure 1b- same as Figure 1a, but for broader TH (km) range (every 3rd TH) and covering from the γ band (barely perceptible) to beyond the *A* band.

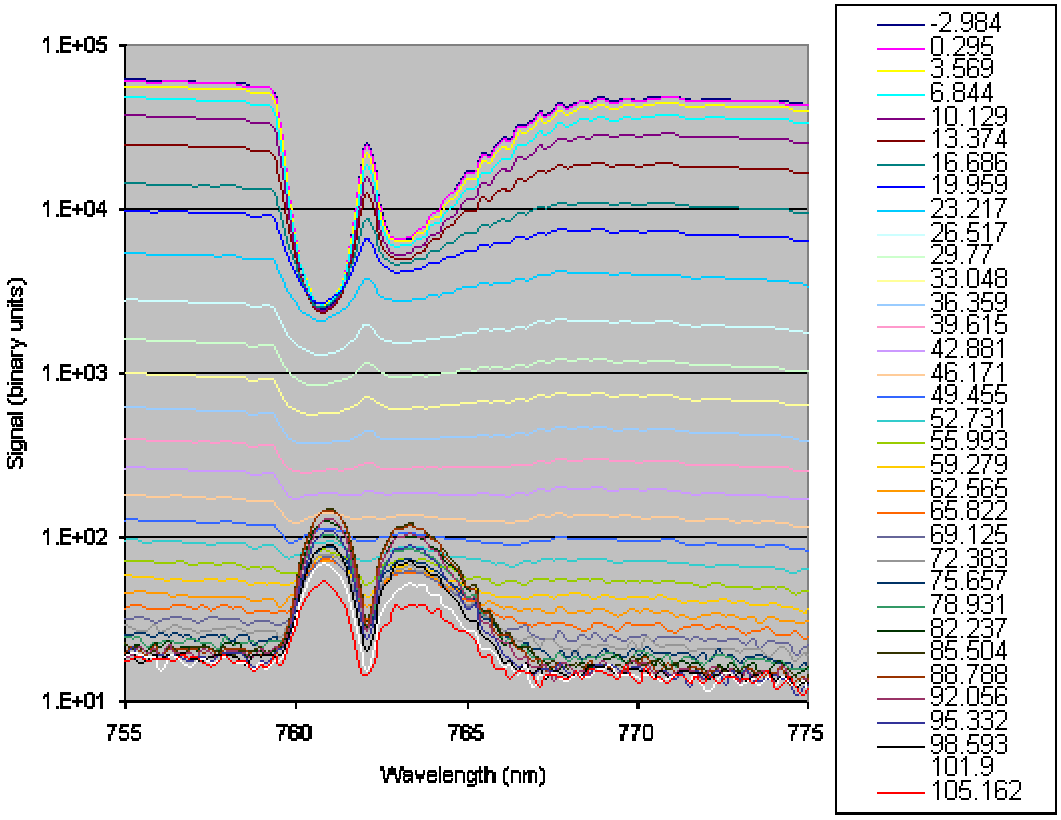

Figure 1c- Spectral signal observed by SCIAMACHY in limb viewing geometry vs. TH (km). The signal is co-added for the 4 azimuthal positions on each TH step. Observation conditions were SZA≅45° (10 am LT), 54° N, August 23rd, 2002.

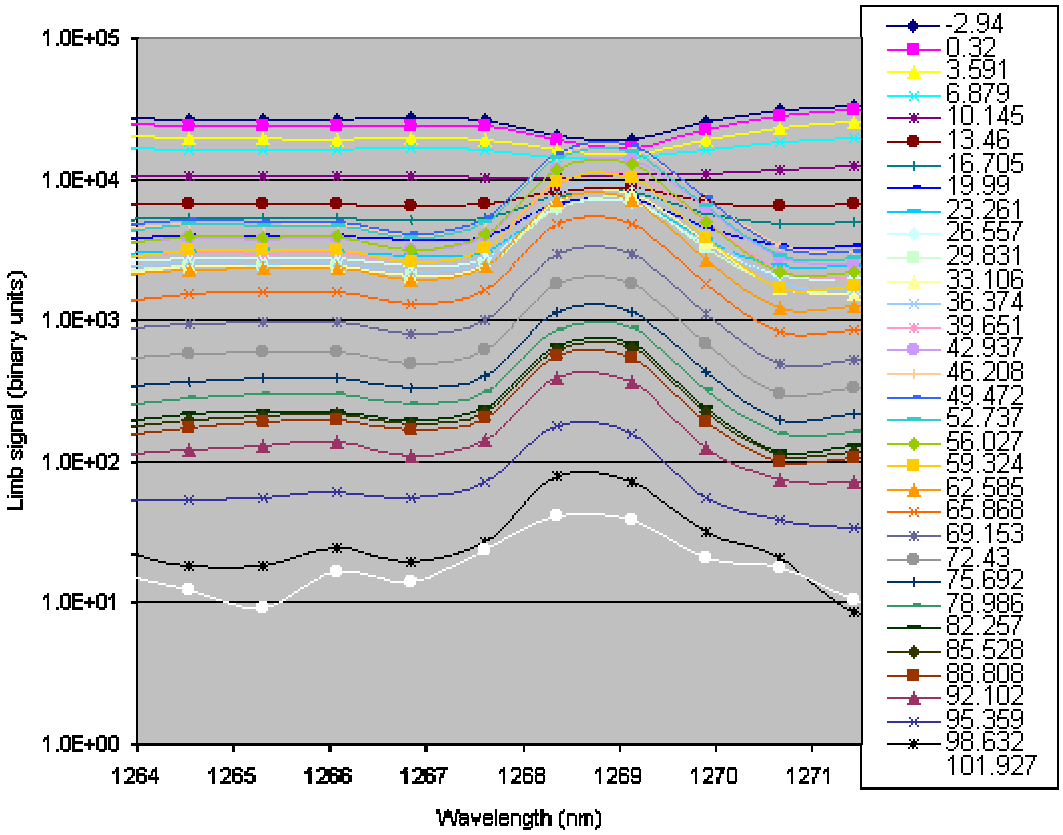

Figure 1d- Limb spectra in the region of the $^1\Delta$ band vs. TH (km) from SCIAMACHY at ~45.5° N, SZA=69.5°, 10 am LT, Jan 23rd, 2003 (orbit 4700). SCIAMACHY has a coarse spectral resolution of 1.48 nm between 1000-1750 nm (Bovensmann *et al.*, 1999).

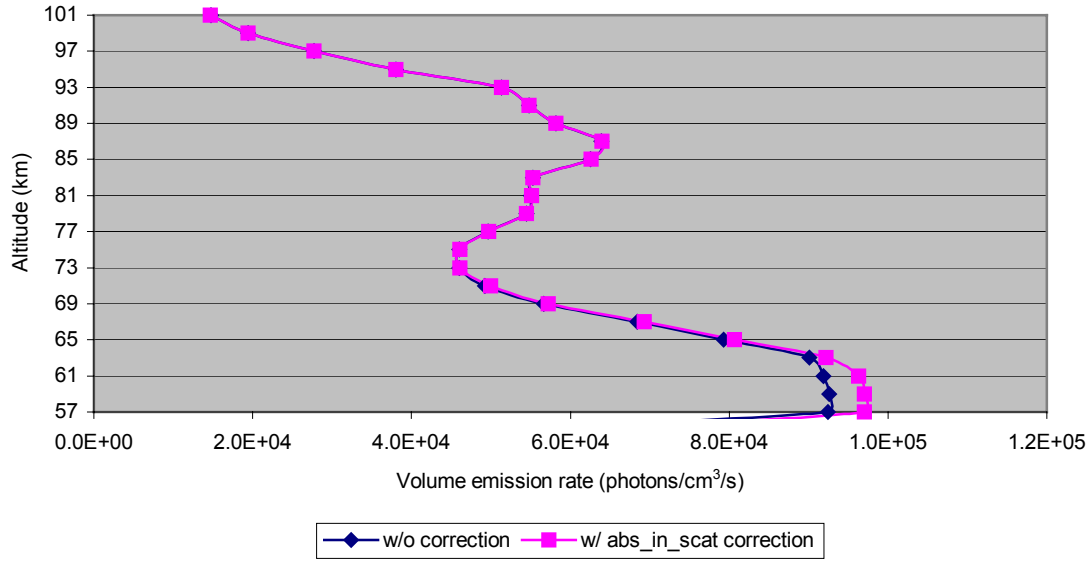

Figure 2- Impact of neglecting correction for O_2 absorption in scattered radiance when analyzing dayglow limb intensity. Naturally, the error increases monotonically with decreasing altitude and reaches 5% at 57 km.

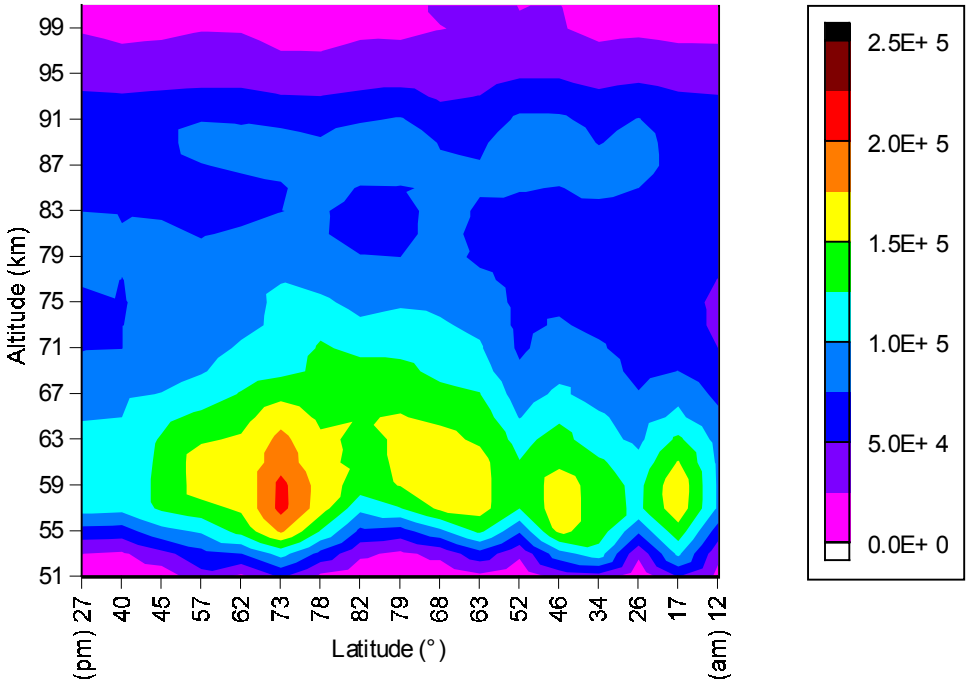

Figure 3- Orbital cross-sectional view of the *A* band dayglow volume emission rate (photons/cm^3/s) on March 16th, 2002 as observed by OSIRIS.

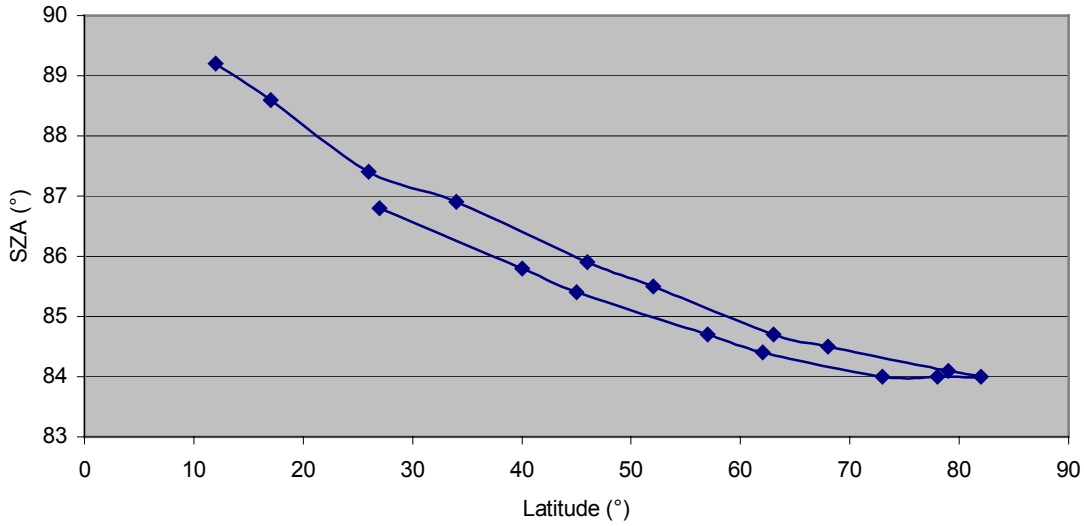

Figure 4- SZA versus latitude. The pm side of the orbit has slightly smaller solar zenith angles on this day.

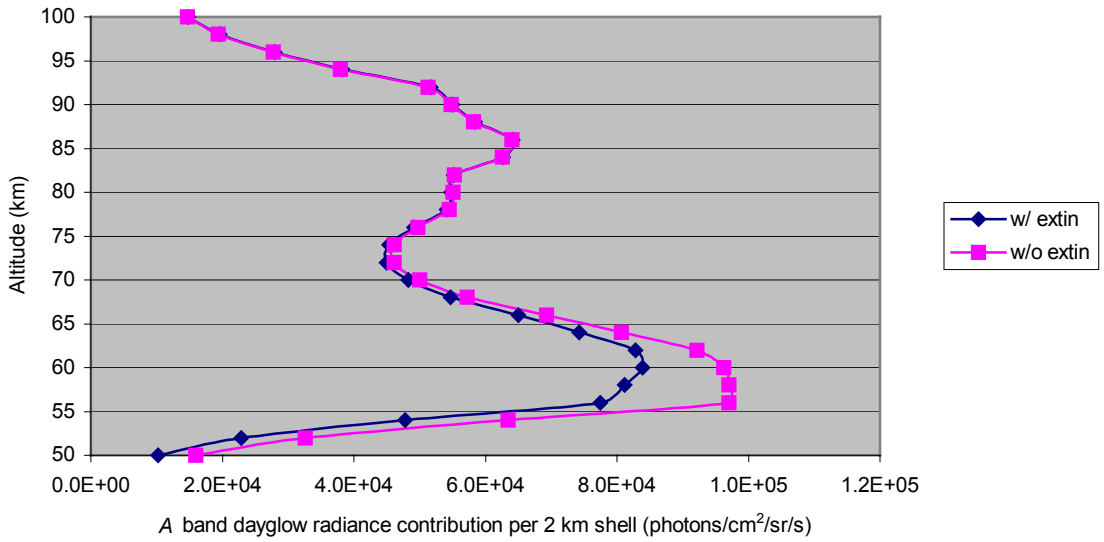

Figure 5a- *A* band dayglow contribution vs. height, with and without extinction along LOS of the nadir viewing instrument.

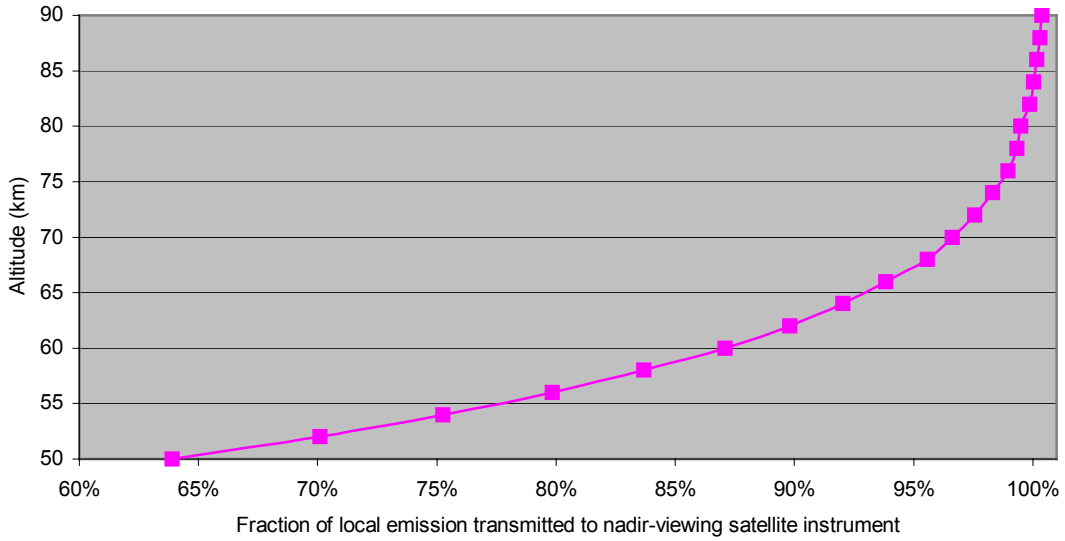

Figure 5b- Proportion of local *A* band emission leaving toward the zenith that transmits to nadir-viewing instrument

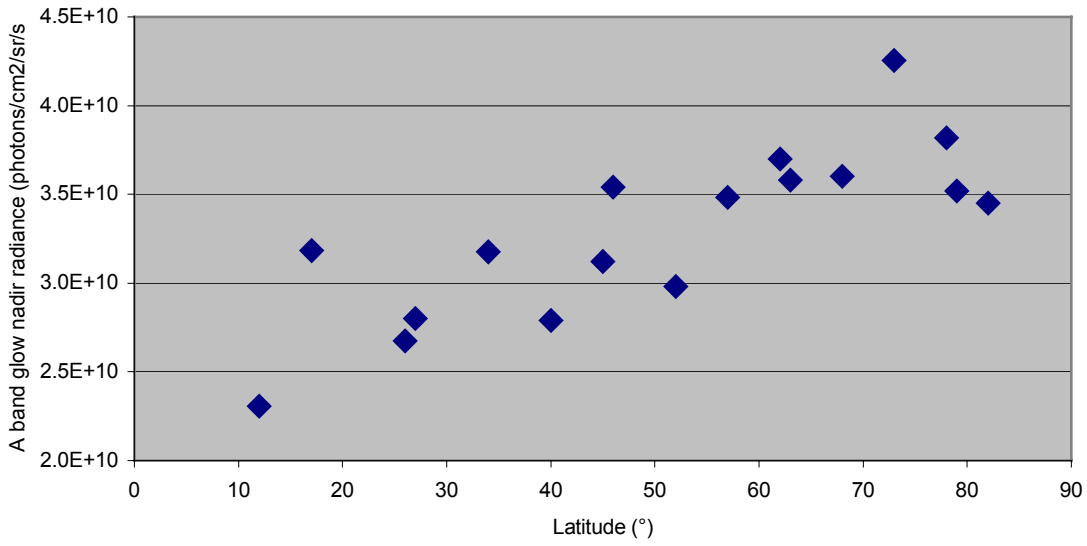

Figure 6- Orbital dependence of nadir radiance due to the dayglow integrated over the *A* band (extinction along nadir LOS is not included, see text for details). The orbit begins at 27° N at ~ 6 pm LT with Odin then ascending to the north pole, where the LT is near noon, and then the descending phase has a local time of ~6 am.

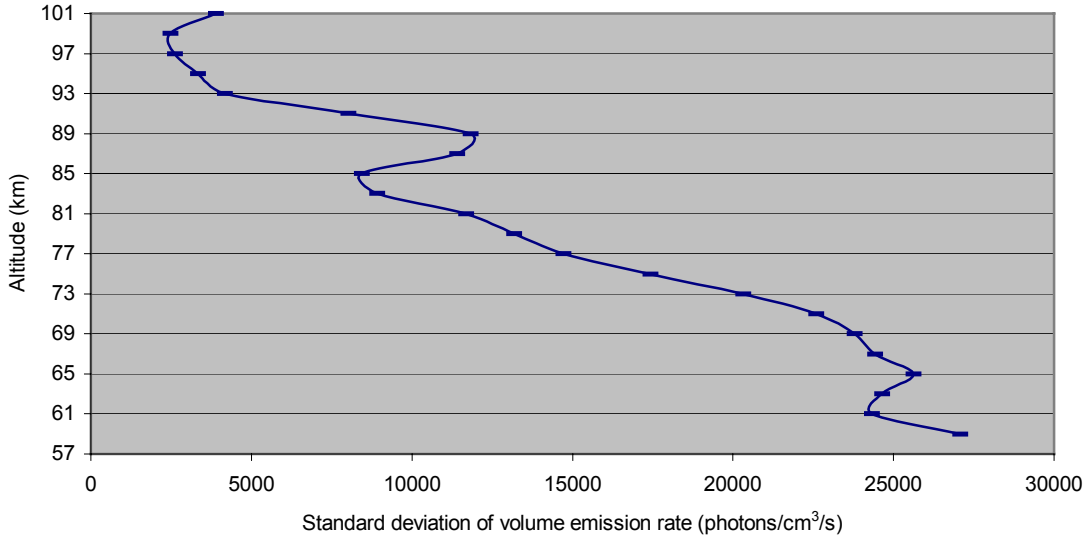

Figure 7a- Variability of volume emission rate as a function of altitude observed by OSIRIS over northern hemisphere, March 16th, 2002 (orbit 11219).

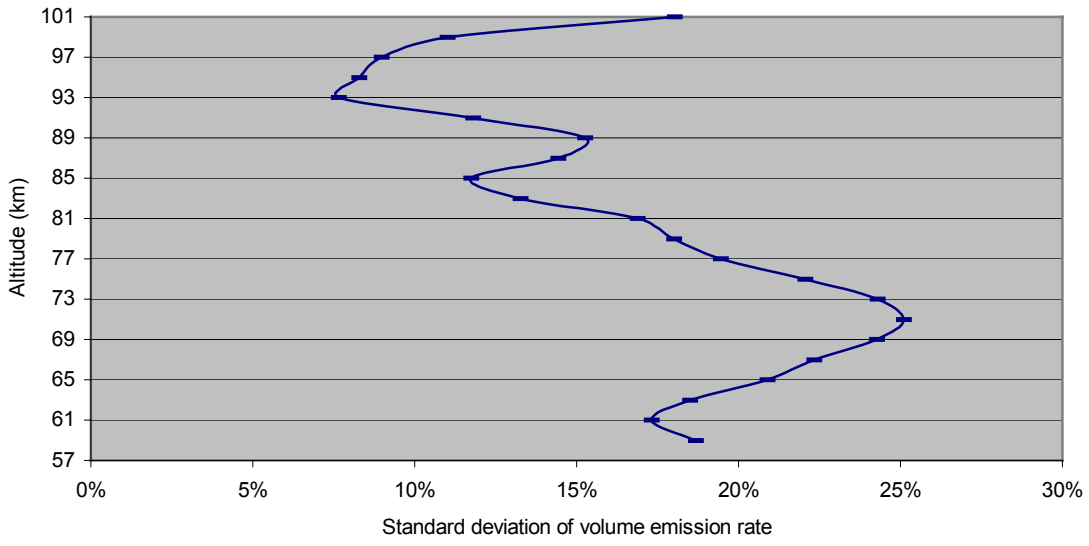

Figure 7b- Variability of volume emission rate, expressed relative to the altitudinal mean over the orbit.

The nadir glow radiance retrieval from limb scan at 78° N during the ascending phase has a local time of 14h35 (± 1h35 as the local time changes quickly over the pole). Thus the local time is very comparable to OCO equator crossing local time. At 78° N, however the local time is much different than at the equator for a sun-synchronous low Earth orbit. However, since the nadir glow radiance varies slowly with latitude, the results at 78° N from OSIRIS are a good approximation for the intensity of the dayglow at mid-latitudes (45° N) for OCO. The nadir glow radiance at 78° N is 3.52e10 photons/s/cm^2/sr, after including the minor correction for the extinction along the LOS.

The nadir glow radiance is converted to a spectral radiance at OCO resolving power, assuming a Gaussian instrumental line profile, by taking the O_2 cross sections at 250 K (a reasonable mesospheric temperature) and iteratively determining a multiplicative constant which would lead to an *A* band nadir radiance of 3.52 e10 photons/s/cm^2/sr, appropriate to 78° N (i.e. OCO local time). The resulting nadir spectral radiance due to the dayglow is shown in Figure 8.

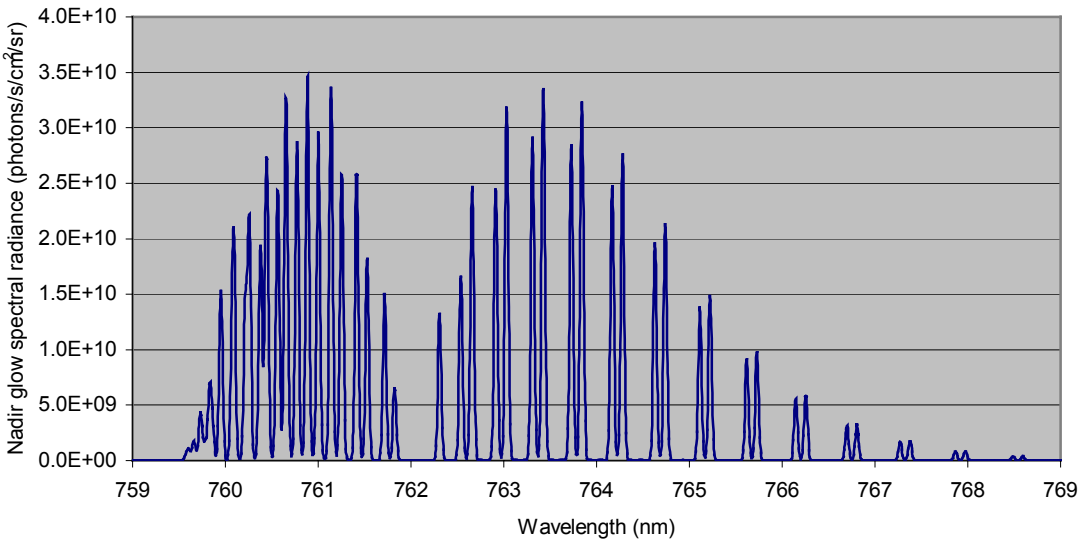

Figure 8- Nadir spectral radiance due to dayglow at OCO resolution and local time (derived from OSIRIS limb radiance observations).

1.2.2 Retrieval of surface pressure with forward model lacking airglow

A "measured" spectrum was generated by adding the nadir glow spectral radiance (Figure 8) to the scattered nadir spectral radiance calculated for the following conditions:

SZA=57.6°
5 orders of scattering (i.e. full multiple scattering)
no aerosols
surface albedo: Λ= 0.1
λ range: 757-771 nm in 0.01 nm steps

Both the glow and scattered contributions to the radiance are appropriate to OCO spectral resolution (resolving power = 18000). The sampling ratio, defined as the number of spectral samplings per FWHM, is 4.2 and is approximately the sampling ratio of OCO (i.e. ~3 [pers. comm. David Crisp]). The effect of spectral binning by the detector has been neglected in this study. A choice of a low surface albedo and no aerosol scattering is chosen to investigate a "worst-case scenario" in terms of airglow contribution to the total radiance. The SZA is typical for OCO at 45° N near equinox.

The retrieval algorithm for the purpose of the airglow sensitivity study consists of a forward radiative transfer model (RTM) nested within a linear regression model. The spectral fit is performed on the same wavelength grid as the forward RTM calculations but only over the range 759.56-769.23 nm since the O_2 absorption signature is mostly contained within this interval. The O_2 column is iteratively adjusted assuming a standard O_2 vertical profile shape until the simulated spectrum best fits the "measured" spectrum.

1.2.3 Results

The retrieved O_2 column, 4.62566±0.00027 $\times 10^{24}$ molec/cm^3, equals the "true" O_2 column (4.62594e24 molec/cm^3), which was used in generating the "measured" spectrum, to within 0.0061%. This bias is two orders of magnitude better than the surface pressure error allowance of OCO of 0.5% [pers. comm., R. J. Salawitch]. The bias is negative because of the filling in of the O_2 absorption lines by the O_2 emission lines (Figures 9-10). The latitudinal bias due to neglecting airglow in the forward RTM is even one order of magnitude smaller since the latitudinal gradient appears to be about ~15% of the total nadir glow radiance (see above). The retrieval bias and uncertainty are small because the retrieval algorithm:

1) fits entire lines but only the line cores have significant residuals due to O_2 emission
2) uses the entire spectral range but the airglow only significantly impacts the strong lines (see Figure 11)

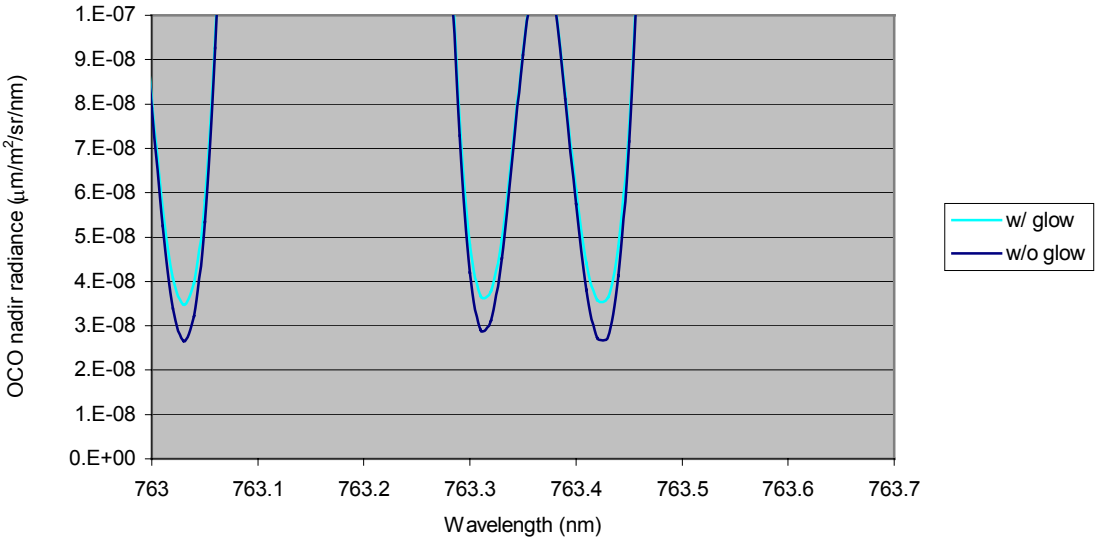

Figure 9- Close-up of the line cores of the *P*7 doublet.

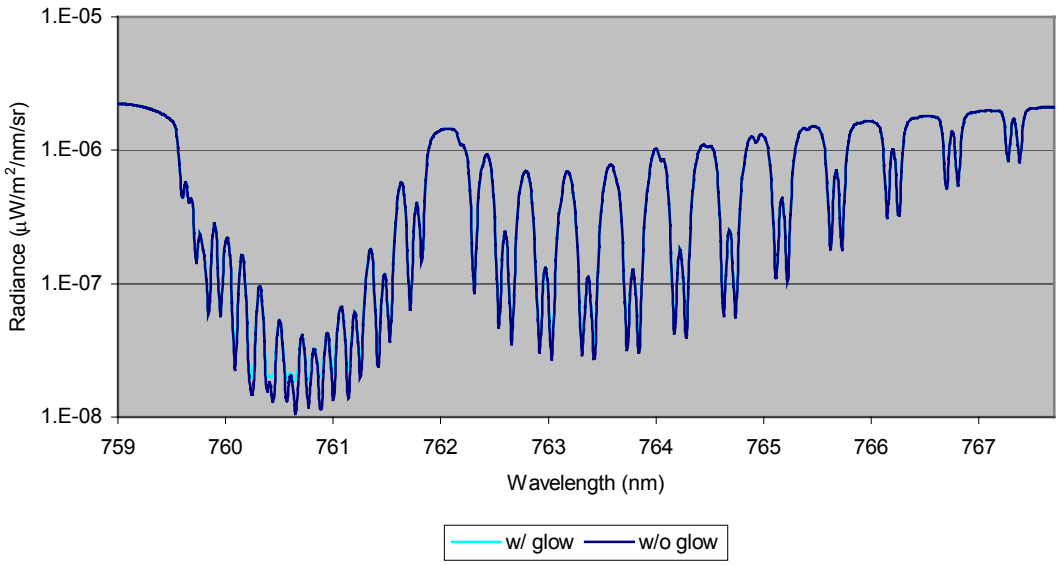

Figure 10- *A* band nadir radiance spectrum at OCO spectral resolution with and without dayglow contribution. Impact of the dayglow is apparent only in the strongest lines where there is minimal radiance due to scattering and maximal radiance contribution due to emission.

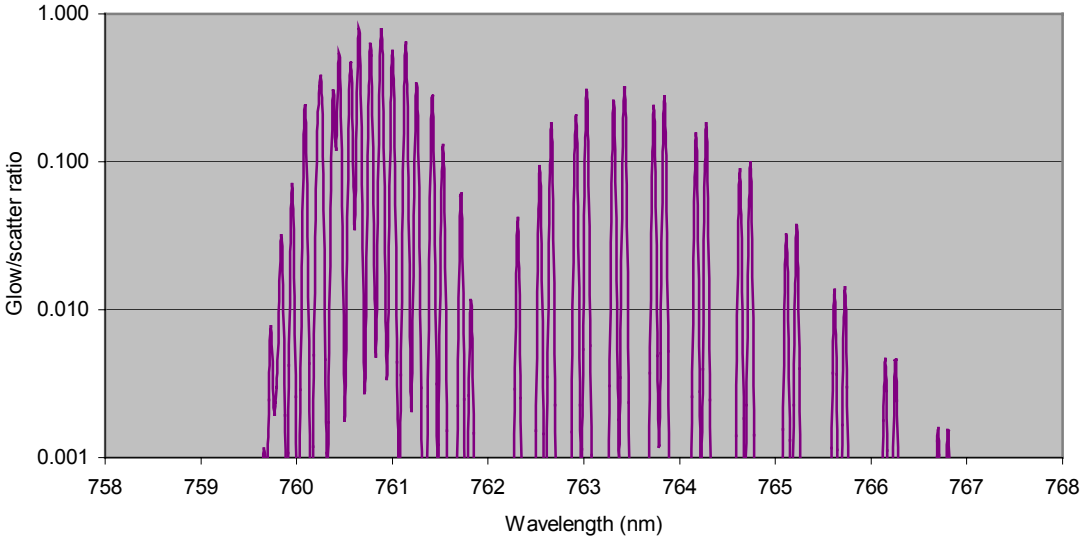

Figure 11- Relative contribution to OCO radiance of O_2 emission versus Rayleigh backscattering and surface reflection. At the core of the strongest *R* branch lines almost half of the total radiance is due to emission.

As a result of the airglow sensitivity study, a retrieval algorithm that limits the retrieval to the wings of weak lines is expected to show the smallest bias due to dayglow. The algorithm applied here fits the continuous spectrum with all spectral points weighted equally.

This study assumes no Doppler shift due to winds (i.e. mesosphere is stationary relative to the surface and the lower atmosphere). The impact of including a Doppler shift in the O_2 emission lines relative to the absorption lines is expected to be negligible particularly at OCO resolution because the typical Doppler shift (assuming 100 km/h wind) is more than 2 orders of magnitude smaller than the OCO resolution and because, as mentioned before, the airglow only significantly impacts very few spectral pixels in the retrieval range.

This sensitivity of surface pressure retrievals to airglow is expected to be approximately independent of surface albedo since only the cores of strong lines are affected by airglow and the incoming radiation at the wavelengths of these line cores does not penetrate to the ground.

2. IMPACT OF THE RING EFFECT

2.1 Background: Ring effect

The Ring effect was named after one of its discoverers, astronomer James Ring, who observed that Fraunhofer lines in spectra of skylight were less deep or "filled in" as compared to the same lines in direct solar spectra [Grainger and Ring, 1962]. Sioris [2001] recently reviewed the literature on the Ring effect. Brinkmann [1968] first correctly explained the main cause of the Ring effect: inelastic rotational Raman scattering (RRS) by N_2 and O_2.

The filling in of molecular absorption bands was observed by Cochran and Trafton [1978], who showed that vibrational Raman scattering and RRS by H_2 fills in the strong infrared and near-IR CH_4 bands on Neptune and Uranus and completely explains the residual intensity in the cores of these bands. Fish and Jones [1995] first observed the filling in of weak telluric NO_2 lines in addition to the filling in of Fraunhofer lines. Sioris [2001] calculated the most accurate RRS cross-sections to date and used them to simulate the Ring effect in the telluric O_2 *A* band (~762 nm) for limb, zenith and nadir geometries [Sioris and Evans, 2000]. They found the effect to be much less than 1% of the continuum radiance in satellite nadir geometry for SZA<89°. The filling in of the *B* band has never been considered.

For satellite nadir geometry, at wavelengths for which the contribution of Rayleigh scattering to the observed intensity dominates over surface reflection (i.e. the ultraviolet and blue), the Ring effect is due almost entirely to rotational Raman scattering. At longer wavelengths, the contribution of plant fluorescence [Sioris *et al.*, 2003] and Rayleigh wing scattering [e.g. Hunten, 1970] by the surface need to be quantified relative to the rotational Raman scattering in the O_2 bands. The Brillouin shifts by ice measured by Amoruso *et al.* [1998] convert to 0.29 cm^{-1} for incident radiation of 760 nm [Young, 1982] and could be significant for the filling in of the *A* band at high spectral resolution (<1 cm^{-1}) at high latitudes.

The impact of the Ring effect on surface pressure retrievals from the O_2 *A* and *B* bands in nadir geometry has never been studied previously. The purpose of this section is to quantify the errors in retrieved surface pressure due to neglecting the Ring effect in the forward radiative transfer model of the retrieval algorithm.

2.2. Method

2.2.1 Calculation of nadir radiance spectrum

The method is described elsewhere [Sioris, 2001; Sioris and Evans, 2000] and will only be highlighted here. The Ring effect is calculated in single scattering mode on a 1 cm^{-1}grid, approaching OCO spectral resolution. Rotational Raman scattering shifts are rounded to the nearest cm^{-1} and extend out to 218 cm^{-1} for N_2. In the line cores, single scattering applies because of strong absorption. In the wings of the lines and in the continuum, the higher order atmospheric scattering term is still ≤10% of the total nadir radiance for an aerosol-free case, regardless of surface albedo. Thus the single scattering approximation appears adequate for Ring effect simulations in aerosol-free cases. Only for such "worst-cases" will the Ring effect lead to a non-trivial bias in the retrieval of surface pressure. When scattering by aerosols contributes strongly to the nadir radiance, the Ring effect will be minimal because this type of scattering is, to a very good approximation, elastic. The *A* band Ring effect calculations are expected to have relative errors of <7% due to the single scattering approximation since multiple scattering only tends to slightly reduce or increase the magnitude of the Ring effect for clear-sky cases depending on the viewing geometry [Sioris, 2001]. Naturally, the *B* band modelling error due to the single scattering approximation is expected to be slightly larger.

The surface reflection is assumed to be elastic and Lambertian and is also included. The atmosphere consists of 32 spherical layers and refraction is included. The temperature profile of the sub-arctic winter atmosphere [Berk *et al.*, 1999] is used for the calculation of the RRS cross sections. The layering is chosen so that the difference in vertical transmittance to space from adjacent layers is always less than 0.10 at all wavelengths. Thus, between the surface (0 km) and 15 km, the layer thickness is 1 km and between 15 and 100 km, the layer thickness is 5 km. The solar spectrum in the *A* band is the Chance-Kurucz solar spectrum from MODTRAN4 [Berk *et al.*, 1999] and has 1 cm^{-1} binning. The following conditions were chosen to maximize the Ring effect contribution (i.e. strong contribution by molecular scattering, low surface albedo):

SZA= 60°
Λ=0.10
no aerosols
A band λ-range: 12918-13182 cm^{-1} (758.61-774.11 nm) in 1 cm^{-1} steps
B band λ-range: 14318-14582 cm^{-1} (685.78-698.42 nm) in 1 cm^{-1} steps

Figure 12 shows the resulting nadir spectra with and without inelastic scattering.

2.2.2A Retrieval of surface pressure from the *A* band with forward model lacking inelastic scattering (RRS): Method and results

The retrieval algorithm concept was described in section 1.2.2.

The retrieval was performed on the same grid as the radiance calculations (see section 2.2.1) but limited to the 13040-13168 cm^{-1} range (759.42-766.87 nm) to focus on the *A* band and not the nearby continuum. The "true" surface pressure is set to 1013.00 mb. The retrieved surface pressure derived from the O_2 column is 1012.54 ± 0.44 mb. The bias was larger than the uncertainty indicating for this case, that the Ring effect, like the dayglow, tends to fill in the O_2 absorption lines (Figures 13-14), leading to a minute, yet systematic underestimation of the surface pressure from the *A* band. Thus the neglect of the frequency-redistributing effects of rotational Raman scattering in the forward model leads to a bias of -0.045% and introduces an uncertainty of 0.044% in the retrieval of surface pressure for Λ=0.10. Both the bias and the uncertainty are more than an order of magnitude smaller than the budgeted surface pressure retrieval error of 0.5%. The Ring effect presumably has a larger impact than the airglow because even though the airglow contributes more strongly in the line core, the Ring effect also impacts the far wings of the O_2 lines (especially for low surface reflectivities as shown below). The small impact of the Ring effect for midday conditions is consistent with the previous findings of Sioris and Evans [2000], who showed that the Ring effect contribution in the *A* band in nadir geometry becomes significant only at near-grazing SZAs when the surface reflection term becomes small.

The impact of the Ring effect has an unexpected dependence on the surface albedo. For a very low surface albedo (Λ<0.03), the dominant effect is that the far wings of the O_2 lines are reduced in the inelastic scattering case as there are rotational Raman ghosts of O_2 line cores superimposed there, leading to a smaller radiance than in the elastic scattering case (see Figures 15-16). Sioris and Evans [2000] also found that the main impact of inelastic RRS in the *A* band was to reduce the intensity in the continuum rather than to fill in the absorption lines. The smaller radiance in the far wings (quasi-continuum) leads the retrieval algorithm to find a higher O_2 column and thus a higher surface pressure. For moderate surface albedo (0.03<Λ<0.1), the Ring effect has very little impact on weak lines and the nearby continuum of the *A* band since the scattering is almost entirely elastic. But the strong lines are filled in by the Ring effect regardless of the surface albedo because the elastically scattering surface does not contribute significantly for these lines. Thus the retrieval bias tends to be negative (i.e. the surface pressure is underestimated). For a highly reflective surface (Λ>0.1), the bias due to the Ring effect decreases with increasing Λ as the elastic scattering from the surface is not entirely absorbed by even the stronger O_2 lines and thus, the filling in of these lines is diluted (see Figure 17) and the retrieval shows a small bias (0.2 mb) in the limit of a bright surface (Λ=1). The retrieval uncertainties increase with decreasing Λ. This is expected since the Ring effect contribution is inversely related to Λ.

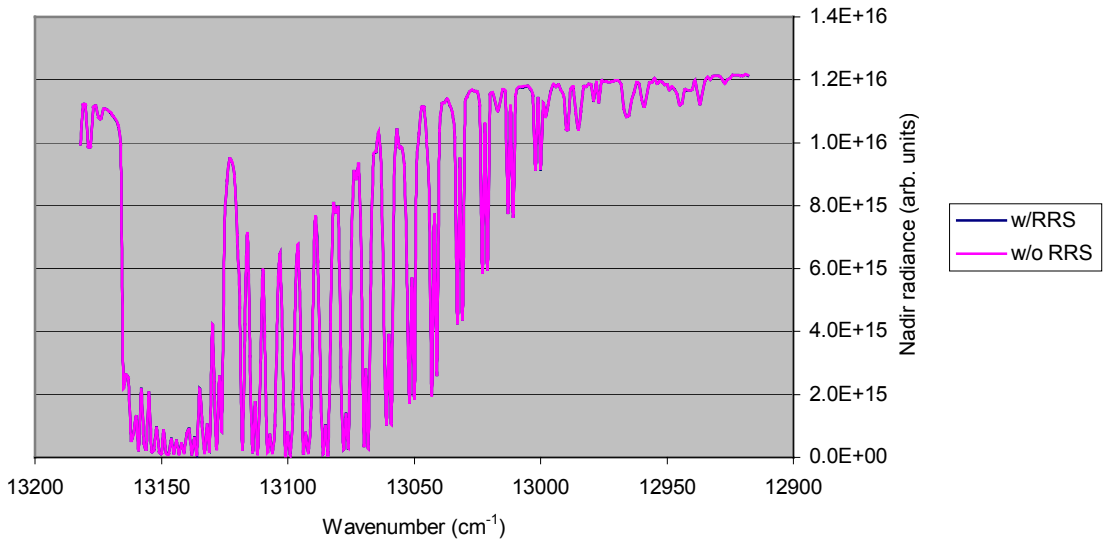

Figure 12- *A* band nadir radiance with and without inelastic scattering (due to RRS) for Λ=0.10. The two curves are almost indistinguishable.

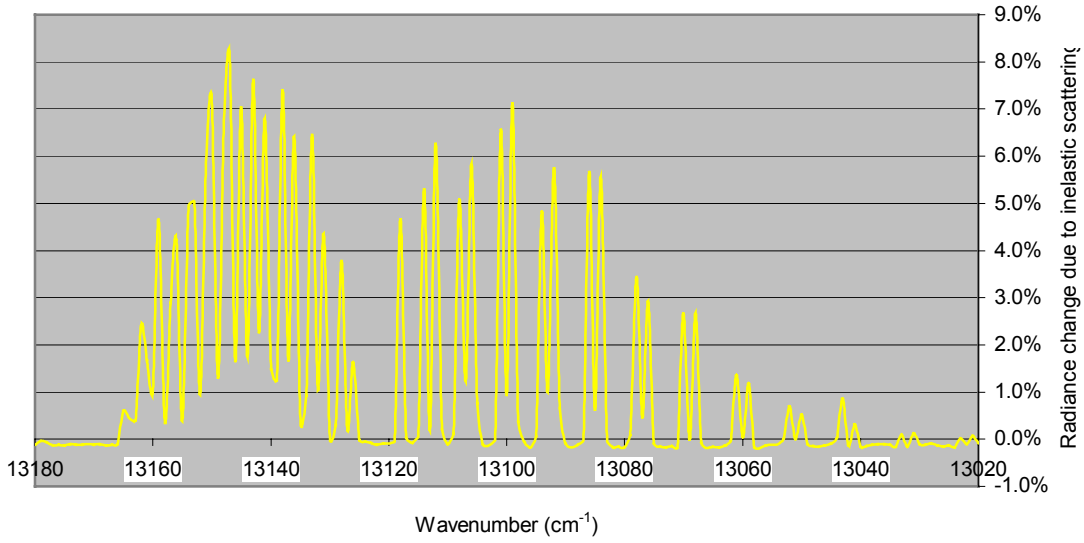

Figure 13- Filling in of the *A* band due to the inelastic component of rotational Raman scattering. The y-axis is the difference in radiance between the elastic and inelastic scattering cases normalized by the inelastic radiance.

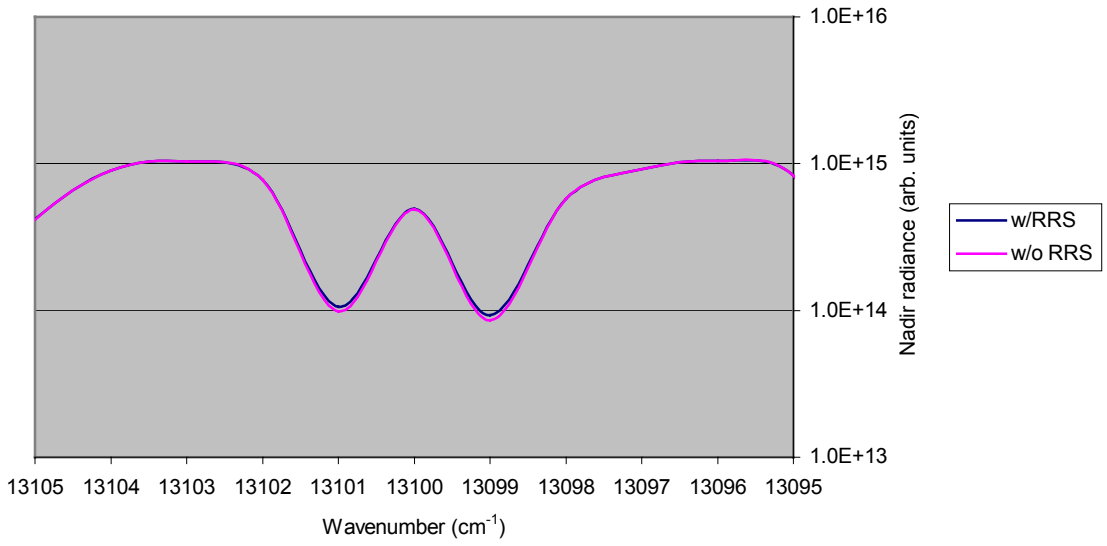

Figure 14- Close-up of the spectrum of *P*7 doublet. Note the scale of the ordinate.

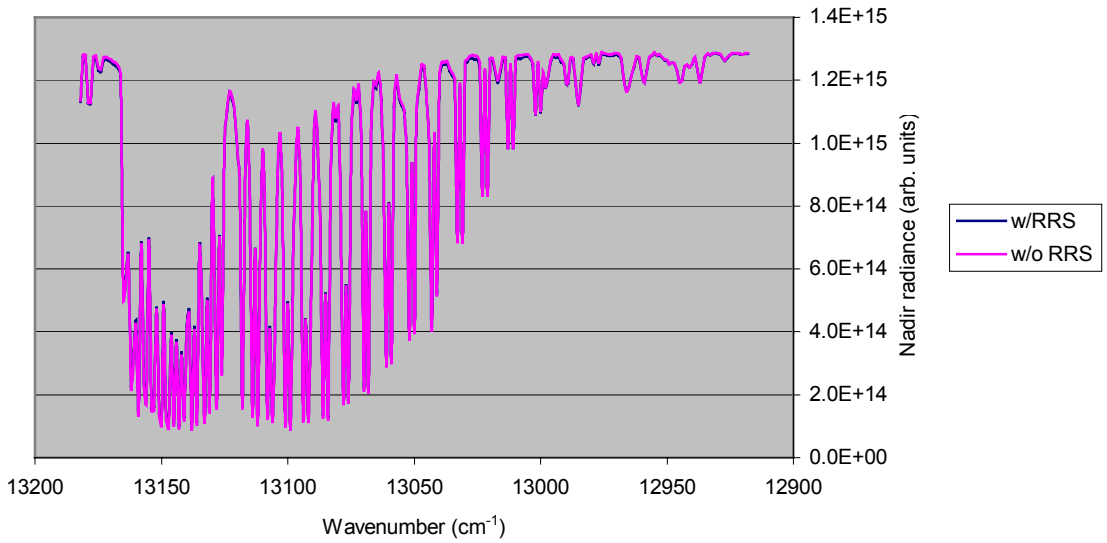

Figure 15- Simulations with and without inelastic scattering for Λ=0.0. Note the reduced continuum value between the high *J* lines of the *P* branch for the purely elastic case.

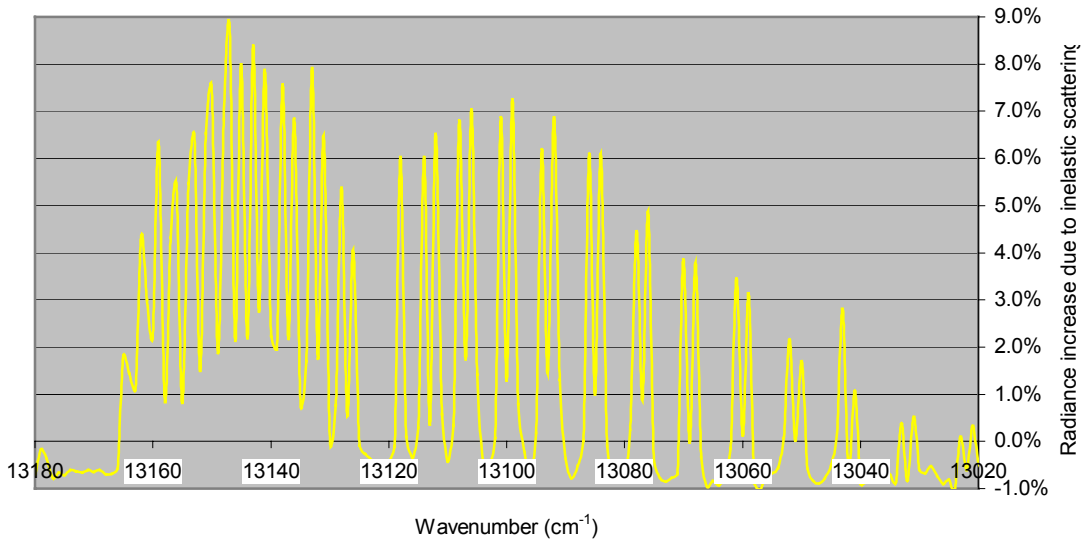

Figure 16- same as Figure 13 but for Λ=0.0. The reduced continuum value between the high *J* lines of the *P* branch is readily apparent and amounts to almost 1% of the total nadir radiance.

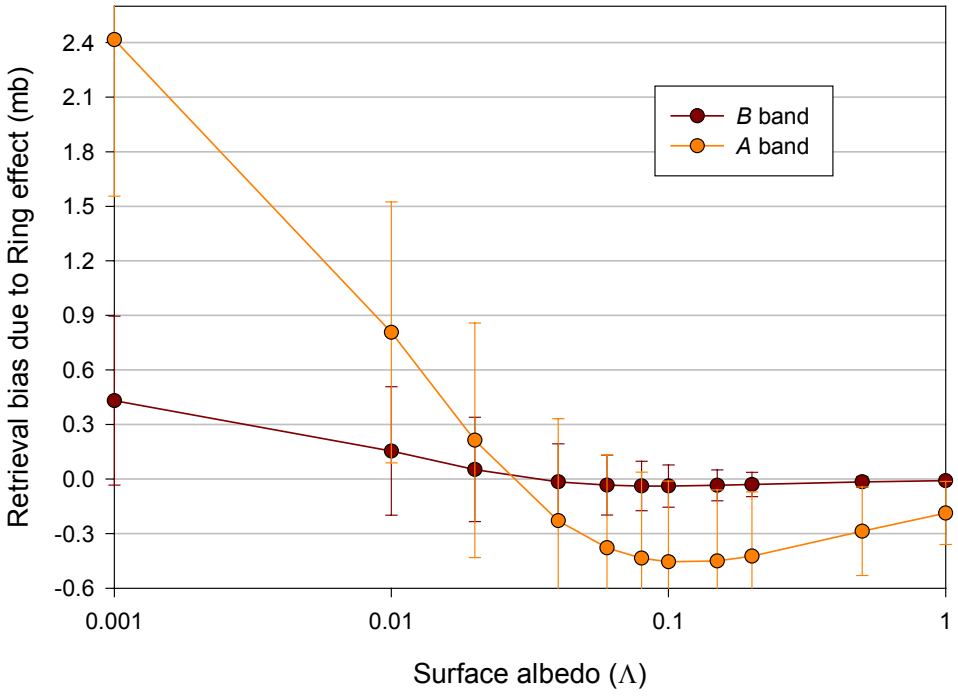

Figure 17- Bias in retrieved surface pressure as a function of surface albedo for SZA=60° and a true surface pressure of 1013.0 mb from two vibronic bands of O_2. The retrieval bias is due to the neglect of inelastic scattering in the forward RTM. At $\Lambda \cong 0.03$, cancelling forward model errors along the *A* band spectrum lead to a minimal surface pressure retrieval bias. The surface albedo of the ocean is ~0.06 at the *A* and *B* bands [McLinden *et al.*, 1997]. The 1-σ retrieval precision is shown as the error bar on the bias. The points at $\Lambda=0.001$ are actually for $\Lambda=0$.

2.2.2B Retrieval of surface pressure from the *B* band with forward model lacking inelastic scattering (RRS)

The radiance calculations (Figure 18) and subsequent spectral fitting analysis was repeated for the *B* band. The 1 cm^{-1} theoretical solar spectrum from R. L. Kurucz (kurucz.harvard.edu/sun/IRRADIANCE/irradiancebins.dat) was used and appears more reliable than in the *A* band based on comparison with other solar spectra (Berk *et al.*, 1999). This is approximately the resolution of OCO (0.81 cm^{-1}) assuming a resolving power of 18000 for the *B* band. Since the filling in in the *A* and *B* band spectral regions is primarily of the O_2 lines and not the Fraunhofer lines, the choice of the solar spectrum is not crucial to the results. The single scattering approximation leads to larger errors in the filling in of the *B* band as multiple scattering contributes in the red part of the spectrum.

For the *B* band, the filling in of the absorption lines is weaker, since the lines are not as deep (Figure 19).

The retrieval range was set to 14424-14560 cm^{-1}(686.81-693.29 nm), analogous to the fitting window of the *A* band. Surface pressure retrieval biases from the *B* band showed the same Λ-dependence as for the *A* band, with the different regimes beginning and ending at similar Λ values (Figure 17). At Λ≅0.04, cancelling errors due to filling in in the line cores and "negative" filling in in the far wings, lead a local minimum in retrieval bias. For darker surfaces, the intensity reduction in the wings prevails and leads to an overestimation of the surface pressure by up to 0.43 mb in the limit of Λ→0.00. For 0.04<Λ<0.1, the biases are negative and reach a maximum bias of -0.04 mb at Λ=0.1 and for bright targets (Λ>0.1), the surface pressure retrieval bias is small and its magnitude decreases monotonically to the Λ→1 limit of -0.009 mb. The amplitude of the bias in the *B* band is considerably reduced relative to the *A* band, particularly for high Λ, since surface reflection contributes in the line cores more effectively than in the stronger *A* band. The fitting uncertainties for the *B* band decrease more rapidly with increasing Λ as the absorption lines of this vibrational overtone are much weaker allowing for greater dilution of the Ring effect by the elastic surface reflection than the fundamental (*A* band).

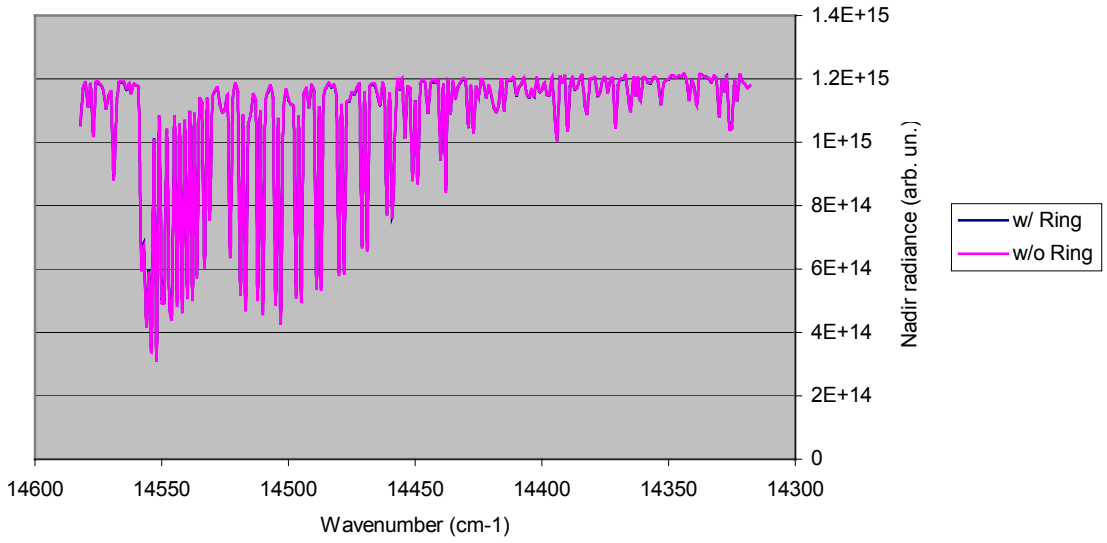

Figure 18- same as Figure 15 but for *B* band (1←0). Notice the lines are not as saturated and that the continuum to the red is slightly less reduced with inelastic scattering than for the *A* band (see Figure 19 also).

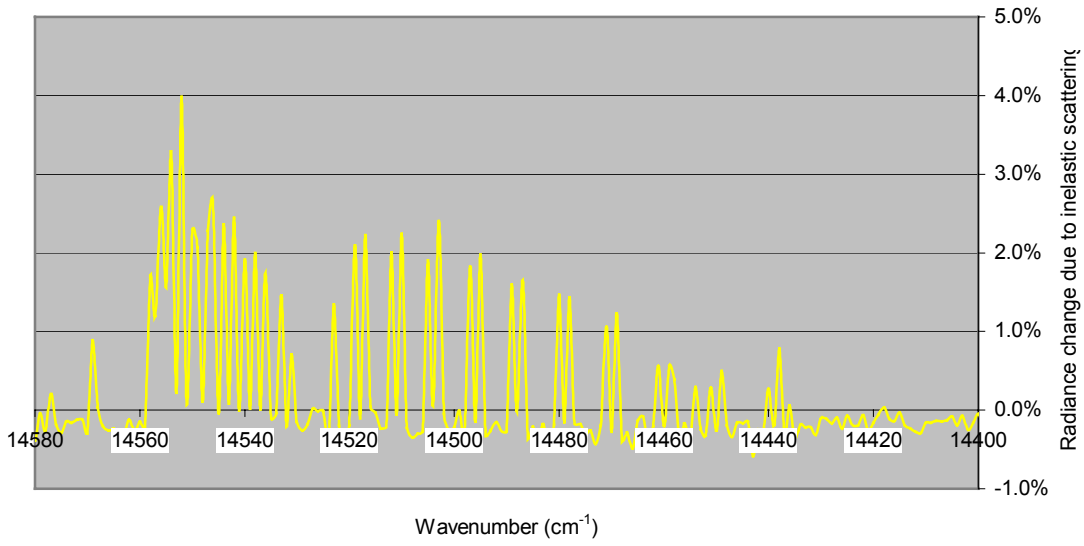

Figure 19- Radiance increase in the *B* band due to the inclusion of inelastic scattering (analogous to Figure 16 for the *A* band).

Conclusions

As a result of this study, two atmospheric effects, namely the dayglow and the Ring effect, are no longer a concern for OCO if a full spectrum fitting approach is adopted. Such the method was used and outlined here to retrieve surface pressures with precisions of <0.4 mb even under worst-case scenarios. The surface pressure retrieval is more sensitive to the neglect of the Ring effect than the dayglow. This is because almost the entire spectrum is slightly distorted by inclusion of inelastic scattering (since RRS occurs at all wavelengths). The *A* band line cores and far wings are particularly affected, in opposite ways from each other, leading to an interesting dependence of the surface pressure retrieval bias on the surface albedo. For the dayglow, the line cores are affected drastically, but the rest of the *A* band is unaffected by the inclusion of this upper atmospheric phenomenon and the retrieval biases and uncertainties are negligible. Based on OSIRIS observations, the orbital variability of the dayglow appears to be due in large part to the orbital (diurnal and latitudinal) variation of mesospheric ozone.

A fitting algorithm that assigns a low weight to the line cores is recommended; otherwise large fitting residuals can be expected, particularly due to dayglow.

Acknowledgments

The author appreciates the comments of Profs. E. J. Llewellyn, I. McDade and D. Gattinger on an earlier draft of this report and thanks to Chris McLinden for providing his state-of-the-art nadir RTM with line-by-line capability for use in the airglow study presented above.

References

Abreu, V. J., A. Bucholtz, P. B. Hays, D. Ortland, W. R. Skinner, J. H. Yee, Absorption and emission line shapes in the O_2 atmospheric bands: Theoretical model and limb viewing simulations, *Appl. Opt.*, **28**, 2128-2137, 1989.

Amoruso, A., P. Benassi, L. Crescentini, and V. Mazzacurati, Low-frequency Raman scattering in normal and deuterated ice I_h, *Phys. Rev. B*, **57**, 7415-7418.

Berk, A., G. P. Anderson, P. K. Acharya, J. H. Chetwynd, L. S. Bernstein, E. P. Shettle, M. W. Matthew, S. M. Adler-Golden, MODTRAN4 User's Manual. Software Manual, Air Force Research Laboratory, Space Vehicles Directorate, Air Force Material Command, Hanscom AFB, MA, 1999.

Bovensmann, H., J. P. Burrows, M. Buchwitz, J. Frerick, S. Noël, V. V. Rozanov, K. V. Chance, A. P. H. Goede, SCIAMACHY: Mission objective and measurement Modes, *J. Atmos. Sci.*, **56**, 127-150, 1999.

Brinkmann, R. T., Rotational Raman scattering in planetary atmospheres, *Astrophys. J.*, **154**, 1087-1093, 1968.

Bucholtz, A., W. R. Skinner, V. J. Abreu, and P. B. Hays, The dayglow of the O_2 atmospheric band system, *Planet. Space Sci.*, **34**, 1031-1035, 1986.

Chahine, M. T., Inverse problems in radiative transfer: Determination of atmospheric parameters, *J. Atmos. Sci.*, *27*, 960-967, 1970.

Cochran, W. D. and L. M. Trafton, Raman scattering in the atmospheres of the major planets, *Astrophys. J.*, **219**, 756-762, 1978.

Gamache, R. R., A. Goldman, L. S. Rothman, Improved spectral parameters for the three most important isotopomers of the oxygen molecule, *J. Quant. Spectrosc. Radiat. Transfer*, **59**, 495-509, 1998.

Grainger, J. R., and J. Ring, Anomalous Fraunhofer line profiles, *Nature,* **193**, 762, 1962.

Heller, J. W., A. B. Christensen, J. H. Yee, and W. H. Sharp, Mesospheric temperature inferred from daytime observation of the O_2 atmospheric (0,0) band system, *J. Geophys. Res.*, **96**, 19499-19505, 1991.

Hunten, D. M., Surface albedo and the filling-in of Fraunhofer lines in the day sky, *Astrophys. J.*, **159**, 1107-1110, 1970.

Marsh, D. R., W. R. Skinner, V. A. Yudin, Tidal influences on O_2 atmospheric band dayglow: HRDI observations vs. model simulations, *Geophys. Res. Lett.*, **26**, 1369-1372, 1999.

Marsh, D. R., W. R. Skinner, A. R. Marshall, P. B. Hays, D. A. Ortland, J.-H. Yee, High Resolution Doppler Imager observations of ozone in the mesosphere and lower

thermosphere, *J. Geophys. Res.*, **107**(D19), 4390, doi:10.1029/2001JD001505, 2002.

McLinden, C. A., D. J. Chartrand, E. Griffioen, J. C. McConnell, and C. T. McElroy, The impact of non-lambertian reflecting surfaces on stratospheric radiation and photochemistry, *J. Atmos. Chem.*, **26**, 29-64, 1997.

McLinden, C. A., J. C. McConnell, E. Griffioen, and C. T. McElroy, A vector radiative transfer model for the Odin/OSIRIS project, *Can J. Phys.*, **80**, 375-393, 2002.

Mlynczak, M. G., F. Morgan, J.-H. Yee, P. Espy, D. Murtagh, B. Marshall, F. Schmidlin, Simultaneous measurements of the $O_2(^1\Delta)$ and $O_2(^1\Sigma)$ airglows and ozone in the daytime mesosphere, *Geophys. Res. Lett.*, **28**, 999-1002, 2001.

Sioris, C. E., G. Bazalgette Courrèges-Lacoste, and M.-P. Stoll, Filling in of Fraunhofer lines by plant fluorescence: Simulations for a nadir-viewing satellite-borne instrument, *J. Geophys. Res.*, **108**(D4), 4133, doi:10.1029/2001JD001321, 2003.

Sioris, C. E., and W. F. J. Evans, Impact of rotational Raman scattering in the O2 *A* band, Geophys. Res. Lett., **27**, 4085–4088, 2000.

Sioris, C. E., The filling in of absorption lines in sky spectra due to rotational Raman scattering, Ph. D. thesis, 135 pp., York University (Toronto), May 2001.

Wallace, L., and D. M. Hunten, Dayglow of the Oxygen A Band, *J. Geophys. Res.*, **73**, 4813-4834, 1968.

Young, A. T., Rayleigh scattering, *Phys. Today,* **35,** 42-48, 1982.